2023 IEEE International Conference on Power Electronics, Smart Grid, and Renewable Energy (PESGRE) | 979-8-3503-1057-3/23/$31.00 ©2023 IEEE | DOI: 10.1109/PESGRE58662.2023.10405381

Modeling and Control of PV and Multiple Batteries based DC Microgrid

Rohan Lalwani
Department of Electrical Engineering
Indian Institute of Technology Roorkee
Email: lalwani_rr@ee.iitr.ac.in

Vishal Kumar
Department of Electrical Engineering
Indian Institute of Technology Roorkee
Email: vishal.kumar@ee.iitr.ac.in

Barjeev Tyagi
Department of Electrical Engineering
Indian Institute of Technology Roorkee
Email: barjeev.tyagi@ee.iitr.ac.in

***Abstract*—This article explores the integration of photovoltaic (PV) systems and multiple Battery Energy Storage Systems (BESSs) through DC-DC converters connected to a common DC bus. It presents an averaged nonlinear model of the converter system, which incorporates a PV system and two distinct BESSs. The model is linearized and validated around a specified operating point. A comprehensive control scheme is discussed that encompasses (i) An outer voltage controller which maintains a constant DC bus voltage, (ii) A battery reference current generation block, and (iii) Inner current controllers which regulate the battery currents or inductor currents to their reference values calculated based on the State of Charges (SOCs). The reference current generation scheme ensures that batteries with a higher SOC discharge at a higher rate and charge at a lower rate, while the opposite is true for batteries with lower SOC. Simulations are conducted in MATLAB/Simulink under varying irradiance and load conditions.**

***Keywords*— Battery Energy Storage Systems, DC-DC Converters, Microgrid Control, State of Charge, System Modeling**

NOMENCLATURE

$\eta_{bi} =$ Efficiency of i^{th} BESS
$\gamma_{b1} =$ Ampere-second rating of i^{th} BESS
$\tilde{q_{bi}} =$ Small signal perturbation duty cycle of S_{bi}
$\tilde{q_{pv}} =$ Small signal perturbation duty cycle of S_{pv}
$i_{bi} =$ Current from i^{th} BESS
$i_{pv} =$ Current from PV
$Q_{bi} =$ Steady state duty cycle of S_{bi}
$q_{bi} =$ Duty cycle of S_{bi}
$Q_{pv} =$ Steady state duty cycle of S_{pv}
$q_{pv} =$ Duty cycle of S_{pv}
$R_{bi} =$ Equivalent series resistance of inductor L_{bi}
$R_c =$ Equivalent series resistance of DC bus capacitor C
$R_o =$ Load resistance
$R_{pv} =$ Equivalent series resistance of inductor L_{pv}
$R_s =$ On state resistance of MOSFET
$v_{bi} =$ Voltage of i^{th} BESS
$v_{bus} =$ DC Bus Voltage
$V_D =$ Diode forward voltage drop
$v_{pv} =$ Solar PV Voltage
$z_{bi} =$ SOC of i^{th} BESS

I. INTRODUCTION

The growing environmental problems caused by burning fossil fuels and the introduction of new loads like electric vehicles necessitate an increase in the use of renewable energy sources (RES) in the electricity grid. Microgrids (MGs) are small-scale power systems that include a group of Distributed Generators (DGs) and loads, offering a promising solution to the current energy crisis [1]. However, integrating more RES into the grid poses challenges such as voltage and frequency fluctuations and stability issues due to the intermittent nature of renewable sources. To address these challenges, energy storage systems (ESS) are seen as a viable solution, serving to mitigate the impact of new power loads and the intermittency of RES. Various types of ESS exist for different grid applications, including voltage regulation, frequency regulation, load leveling, and peak shaving [2].

Battery energy storage systems (BESSs) are the most commonly used ESS due to their cost-effectiveness and quick response. In grid-connected mode, BESS is scheduled to shift energy consumption based on forecasts, thereby reducing the microgrid's operational costs. In islanded or isolated mode, BESS is utilized to maintain power balance by storing excess energy when generation exceeds demand and supplying deficit power when demand exceeds generation [3]. Lead acid batteries, which are mature and affordable, are widely employed in grid applications due to their durability [4]. However, with advancements in technology and cost reduction, other battery technologies such as lithium-ion and redox flow are now available in the market. Utilizing different battery technologies allows for the creation of grid storage systems that combine multiple batteries, enhancing power capacity , reliability, cost-effectiveness, and energy management [4].

A typical microgrid system consisting of multiple batteries and PV is shown in Figure 1.

When multiple batteries of different chemistries are connected to a common DC bus through converters in a DC microgrid system, it becomes crucial to develop current-sharing strategies to ensure optimal charging and discharging. Numerous studies in the literature focus on controlling multiple battery energy storage systems. In one study [4] a dual storage system using two battery banks with different functions and sizes was proposed for isolated microgrids, addressing their complex and variable operation. Another study [5] proposes a battery power system with parallel operation of BESSs, offering advantages such as flexible design, improved reliability, efficient energy utilization, and simplified maintenance.

979-8-3503-1057-3/23/$31.00 ©2023 IEEE.

A power sharing method in a DC microgrid was presented in a study [6] to achieve state of charge (SOC) balancing among distributed battery energy units (BEUs). Accurate power sharing is achieved by dynamically adjusting the virtual power ratings of BEUs based on their SOC levels. Similarly, another paper [7] presents a battery energy management strategy for a microgrid system with PV and DGs. The proposed system reduces fossil fuel consumption, mitigates PV power fluctuations, and extends battery life cycle. It considers multiple battery types and achieves various management objectives.

To address the limitations of conventional droop control, an improved strategy using SOC-based droop coefficients was proposed in a study [8]. Another work [9] for a DC microgrid with PV and multiple BESS. It incorporates SOC adaptive DC power droop control for bidirectional DC-DC converters, enhancing battery life and enabling decentralized load power sharing. A dual loop non-linear control structure combining interconnection damping assessment-passivity based controller and finite control set-model predictive controller was proposed in a study [10] for a PV, battery, and supercapacitor-based standalone DC microgrid.

Furthermore, an adaptive nonlinear droop control technique for distributed battery energy storage systems in DC microgrids was proposed in a study [11], achieving balanced load-sharing and precise voltage regulation based on battery SOC. An adaptive multi-agent model-free iPI control strategy for SOC balancing in super-UPS was presented in another paper [12], demonstrating superior control performance over traditional PI control.

Authors in [13] modeled the system consisting of multiple batteries and reviews various droop control schemes. Furthermore, it proposes a new droop control method for PV grid-interactive DC microgrid with two BESSs.

Additional studies focus on optimization frameworks, electrical modeling, power flow control methods, and integration of hybrid batteries. These include papers on modeling and optimization of battery-supercapacitor hybrid electrical energy storage systems [14], accurate electrical modeling for batteries [15], power flow control methods for multiple battery converters [16], operational modes of modular multilevel converters for integrating hybrid batteries [17], reducing battery degradation costs in islanded DC microgrids [18], SOC balancing schemes using droop control strategies [19] and comparing droop control methods for SOC balancing of BESSs in islanded DC microgrids [20], and load sharing methods in distributed microgrid systems for balancing SOC among parallel connected batteries [21].

These research papers collectively contribute to the advancements in battery energy storage systems and their control strategies, addressing the challenges associated with integrating renewable energy sources into microgrids with multiple batteries.

This paper's contributions encompass the development and validation of both nonlinear and linear models consisting of multiple batteries, the exploration of the current sharing strategy based on SOC of different batteries, and the discussion of control of DC bus voltage and battery currents. These findings contribute to the advancement of power converter systems and facilitate the integration of PV and multiple batteries in renewable energy applications.

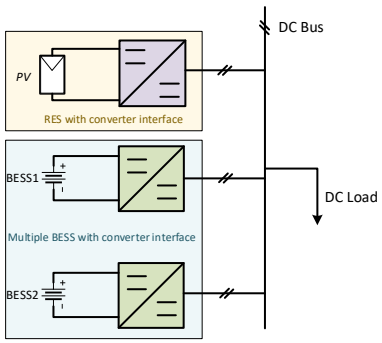

Fig. 1. Typical DC Microgrid System

The remaining paper is organized as follows. In section II, a typical system consisting of multiple batteries is mathematically modeled and linearized model is validated. Section III describes control scheme and current sharing strategy for multiple BESS. In section IV simulation results have been discussed for varying irradiance and load conditions. Section V includes the concluding remarks.

II. Modeling and Validation

The studied system has shown in the figure 2. It comprises a PV, Li-ion (BESS1), and Lead acid (BESS2) battery connected with a DC bus through a DC-DC boost converter and bi-directional DC-DC converters.

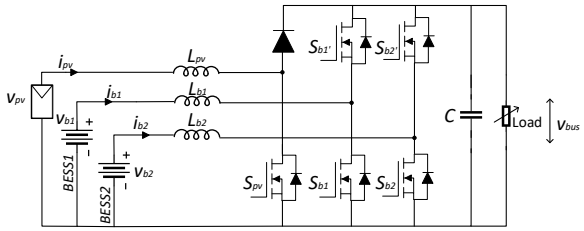

Fig. 2. Studied System

A. Modeling

Individual converter's on-time and off-time state equations have been written, and the averaged large signal model has been developed, expressed by the following equations.

1) Converter Modeling:

$$\left\langle \frac{di_{pv}}{dt} \right\rangle = \frac{v_{pv}}{L_{pv}} - \left(\frac{R_{pv} + R_s q_{pv} + R_p (1 - q_{pv})}{L_{pv}} \right) i_{pv} - \left(\frac{R_p (1 - q_{b1})(1 - q_{pv})}{L_{pv}} \right) i_{b1} - \left(\frac{R_p (1 - q_{b2})(1 - q_{pv})}{L_{pv}} \right) i_{b2} - \left(\frac{R_p (1 - q_{pv})}{R_c L_{pv}} \right) v_c - \frac{(1 - q_{pv})}{L_{pv}} V_D \quad (1)$$

$$\left\langle \frac{di_{b1}}{dt} \right\rangle = \frac{v_{b1}}{L_{b1}} - \left(\frac{R_{b1} + R_s q_{b1} + R_p (1 - q_{b1})}{L_{b1}} \right) i_{b1} - \left(\frac{R_p (1 - q_{b1}) (1 - q_{pv})}{L_{b1}} \right) i_{pv} - \left(\frac{R_p (1 - q_{b2}) (1 - q_{b1})}{L_{b1}} \right) i_{b2} - \left(\frac{R_p (1 - q_{b1})}{R_c L_{b1}} \right) v_c - \frac{(1 - q_{b1})}{L_{b1}} V_D \quad (2)$$

$$\left\langle \frac{di_{b2}}{dt} \right\rangle = \frac{v_{b2}}{L_{b2}} - \left(\frac{R_{b2} + R_s q_{b2} + R_p (1 - q_{b2})}{L_{b2}} \right) i_{b2} - \left(\frac{R_p (1 - q_{b2}) (1 - q_{pv})}{L_{b2}} \right) i_{pv} - \left(\frac{R_p (1 - q_{b2}) (1 - q_{b1})}{L_{b2}} \right) i_{b1} - \left(\frac{R_p (1 - q_{b2})}{R_c L_{b2}} \right) v_c - \frac{(1 - q_{b2})}{L_{b2}} V_D \quad (3)$$

$$\left\langle \frac{dv_c}{dt} \right\rangle = \left(\frac{R_p (1 - q_{pv})}{R_c C} \right) i_{pv} + \left(\frac{R_p (1 - q_{b1})}{R_c C} \right) i_{b1} + \left(\frac{R_p (1 - q_{b2})}{R_c C} \right) i_{b2} - \frac{v_c}{(R_o + R_c) C} \quad (4)$$

Where, $v_{bus} = v_c + R_c C \frac{dv_c}{dt}$, $R_p = \frac{R_o R_c}{R_o + R_c}$.

2) Battery Modeling: SOCs of the batteries are related with their currents according to the coulomb count as follows,

$$z_{b1}(t) = z_{b1}(t_o) - \frac{\eta_{b1}}{\gamma_{b1}} \int_{t_o}^{t} i_{b1} dt \quad (5)$$

$$z_{b2}(t) = z_{b2}(t_o) - \frac{\eta_{b2}}{\gamma_{b2}} \int_{t_o}^{t} i_{b2} dt \quad (6)$$

Since it has been observed that second order terms are also present in the averaged state equations, so, the obtained averaged model is nonlinear. Most of the control studies or analytical studies deal with LTI systems. So, to linearize the model, an operating point around which linearization has to be performed must be evaluated. The operating point has been evaluated by plugging the system parameters and steady state values of state variables into the state equations (Equation 1 to 4) and equating them to zero. The system parameters are stated in the Table I. The obtained operating point is mentioned in Appendix A.

So, perturbing the variables about an operating point to linearize it.

$i_{pv} = I_{pv} + \tilde{i_{pv}}$, $i_{b1} = I_{b1} + \tilde{i_{b1}}$, $i_{b2} = I_{b2} + \tilde{i_{b2}}$, $v_c = V_c + \tilde{v_c}$, $z_{b1} = SOC_{b1} + \tilde{SOC_{b1}}$, $z_{b2} = SOC_{b2} + \tilde{SOC_{b2}}$, $v_{bus} = V_{bus} + \tilde{v_{bus}}$, $q_{pv} = Q_{pv} + \tilde{q_{pv}}$, $q_{b1} = Q_{b1} + \tilde{q_{b1}}$, $q_{b2} = Q_{b2} + \tilde{q_{b2}}$

Considering only first order terms, the following state matrices are developed such that,

$$\left[\dot{\tilde{x}}\right]_{6\times1} = [A]_{6\times6} [\tilde{x}]_{6\times1} + [B]_{6\times6} [\tilde{u}]_{6\times1} \quad (7)$$

$$[\tilde{y}]_{3\times1} = [C]_{3\times6} [\tilde{x}]_{6\times1} + [D]_{3\times6} [\tilde{u}]_{6\times1} \quad (8)$$

Where,

$$\tilde{x} = \begin{bmatrix} \tilde{i_{pv}} \\ \tilde{i_{b1}} \\ \tilde{i_{b2}} \\ \tilde{v_c} \\ \tilde{SOC_{b1}} \\ \tilde{SOC_{b2}} \end{bmatrix}, \dot{\tilde{x}} = \begin{bmatrix} \dot{\tilde{i_{pv}}} \\ \dot{\tilde{i_{b1}}} \\ \dot{\tilde{i_{b2}}} \\ \dot{\tilde{v_c}} \\ \dot{\tilde{SOC_{b1}}} \\ \dot{\tilde{SOC_{b2}}} \end{bmatrix}, \tilde{u} = \begin{bmatrix} \tilde{q_{pv}} \\ \tilde{q_{b1}} \\ \tilde{q_{b2}} \\ \tilde{v_{pv}} \\ \tilde{v_{b1}} \\ \tilde{v_{b2}} \end{bmatrix}, \tilde{y} = \begin{bmatrix} \tilde{v_{bus}} \\ \tilde{i_{b1}} \\ \tilde{i_{b2}} \end{bmatrix}$$

And the system matrices are given in Equation 9,10,11.

These models can be extended for the larger system consisting of more number of batteries.

B. Model Validation

Duty cycle and source voltage perturbations are applied to small signal and large signal model. The response of small signal and large signal model perturbed around the operating point has to be same for model to be validated. Duty cycle perturbation around its operating point is applied as $\tilde{q_{pv}} = \tilde{q_{b1}} = \tilde{q_{b2}} = 0.05 \sin(10t)$ and input voltage or source voltage perturbation is applied as $\tilde{v_{pv}} = \tilde{v_{b1}} = \tilde{v_{b2}} = 10 \sin(10t)$. DC bus voltage is observed with perturbed inputs for both the models, it is clear from the validation results shown in Figure 3 that linearized small signal model is following the large signal model when small signal perturbation is applied to both the models. Hence, small signal model is validated.

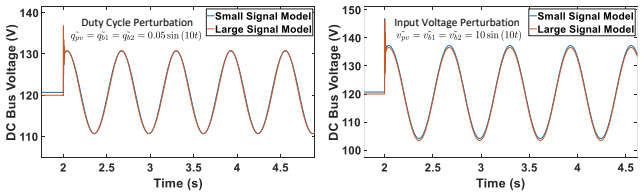

Fig. 3. Model Validation Results

III. Control of Studied Converter

A. Control Scheme

This article proposes the control scheme shown in Figure 4. The outer voltage control loop is designed to maintain the DC bus voltage constant at a reference of $120V$. The error of DC bus voltage $(v_{bus}(ref) - v_{bus})$ is processed through a PI controller, which results in total current from batteries $i_b(ref)$. Now, current $i_b(ref)$ is the sum of currents from both batteries. Inner current controllers require individual reference currents of both batteries. A reference current generation block is incorporated to generate the individual reference currents $i_{b1}(ref)$ and $i_{b2}(ref)$. These reference currents are then compared with the actual currents from the batteries i_{b1} and i_{b2}, and errors are processed through their respective PI controllers. The outputs of the PI controllers are the duty cycles of the respective battery converters. PWM generation

$$A=\begin{bmatrix} \frac{-\left(R_{pv}+R_sQ_{pv}+R_pQ'_{pv}\right)}{L_{pv}} & \frac{-R_pQ'_{b1}Q'_{pv}}{L_{pv}} & \frac{-R_pQ'_{b2}Q'_{pv}}{L_{pv}} & \frac{-R_pQ'_{pv}}{R_cL_{pv}} & 0 & 0 \\ \frac{-R_pQ'_{b1}Q'_{pv}}{L_{b1}} & \frac{-\left(R_{b1}+R_sQ_{b1}+R_pQ'_{b1}\right)}{L_{b1}} & \frac{-R_pQ'_{b2}Q'_{b1}}{L_{b1}} & \frac{-R_pQ'_{b1}}{R_cL_{b1}} & 0 & 0 \\ \frac{-R_pQ'_{b2}Q'_{pv}}{L_{b2}} & \frac{-R_pQ'_{b2}Q'_{b1}}{L_{b2}} & \frac{-\left(R_{b2}+R_sQ_{b2}+R_pQ'_{b2}\right)}{L_{b2}} & \frac{-R_pQ'_{b2}}{R_cL_{b2}} & 0 & 0 \\ \frac{R_pQ'_{pv}}{R_cC} & \frac{R_pQ'_{b1}}{R_cC} & \frac{R_pQ'_{b2}}{R_cC} & -\frac{1}{(R_c+R_o)C} & 0 & 0 \\ 0 & \frac{\eta_{b1}}{\gamma_{b1}} & 0 & 0 & 0 & 0 \\ 0 & 0 & \frac{\eta_{b2}}{\gamma_{b2}} & 0 & 0 & 0 \end{bmatrix} \tag{9}$$

$$B=\begin{bmatrix} \frac{\alpha_{pv}}{L_{pv}} & \frac{R_pI_{b1}Q'_{pv}}{L_{pv}} & \frac{R_pI_{b2}Q'_{pv}}{L_{pv}} & \frac{1}{L_{pv}} & 0 & 0 \\ \frac{R_pI_{pv}Q'_{b1}}{L_{b1}} & \frac{\alpha_{b1}}{L_{b1}} & \frac{R_pI_{b2}Q'_{b1}}{L_{b1}} & 0 & \frac{1}{L_{b1}} & 0 \\ \frac{R_pI_{pv}Q'_{b2}}{L_{b2}} & \frac{R_pI_{b1}Q'_{b2}}{L_{b2}} & \frac{\alpha_{b2}}{L_{b2}} & 0 & 0 & \frac{1}{L_{b2}} \\ \frac{-R_pI_{pv}}{R_cC} & \frac{-R_pI_{b1}}{R_cC} & \frac{-R_pI_{b2}}{R_cC} & 0 & 0 & 0 \\ 0 & 0 & 0 & 0 & 0 & 0 \\ 0 & 0 & 0 & 0 & 0 & 0 \end{bmatrix} \tag{10}$$

$$C=\begin{bmatrix} R_pQ'_{pv} & R_pQ'_{b1} & R_pQ'_{b2} & \frac{R_p}{R_c} & 0 & 0 \\ 0 & 1 & 0 & 0 & 0 & 0 \\ 0 & 0 & 1 & 0 & 0 & 0 \end{bmatrix}, D=\begin{bmatrix} R_pI_{pv} & R_pI_{b1} & R_pI_{b2} & 0 & 0 & 0 \\ 0 & 0 & 0 & 0 & 0 & 0 \\ 0 & 0 & 0 & 0 & 0 & 0 \end{bmatrix} \tag{11}$$

block compares the duty cycle with a triangular or sawtooth wave and generates the pulses which can be applied to the switches S_{b1} and S'_{b1} for BESS1 and S_{b2} and S'_{b2} for BESS2. P&O algorithm has been used to generate the duty cycle for switch S_{pv} to operate the PV in Maximum Power Point Tracking (MPPT) mode.

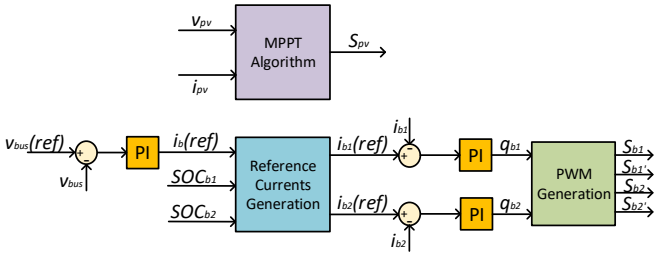

Fig. 4. Control scheme

B. Reference Current Generation

Let there be N number of batteries connected to a DC bus through N number of converters. $i_b(ref)$ generated by the outer voltage controller is to be divided among these batteries. The current sharing among multiple BESSs can be done considering various battery parameters such as SOC, internal resistance, temperature, cost, life cycles, etc. This article mainly focuses on current sharing based on the SOCs of the batteries. Here, the convention is, discharging of the battery is represented by a positive current and charging by a negative current. Now, if $i_b(ref) > 0$, batteries need to discharge, and their discharge currents should be directly proportional to their SOCs. Hence, during discharge j^{th} battery reference current can be represented by $i_j\,(ref) = \frac{SOC_j}{\sum_{n=1}^{N} SOC_n} i_b\,(ref)$. if $i_b(ref) < 0$, batteries would go into charging mode, and it is desired to charge the batteries with currents inversely proportional to their SOCs i.e. the battery with the least SOC should charge at higher currents. Hence, during discharge j^{th} battery reference current can be represented by $i_j\,(ref) = \frac{\frac{1}{SOC_j}}{\sum_{n=1}^{N} \frac{1}{SOC_n}} i_b\,(ref)$. These generated reference currents are applied at inner current controllers as shown in the control scheme block diagram of Figure 4. The flowchart of current sharing based on SOCs of batteries is shown in Figure 5.

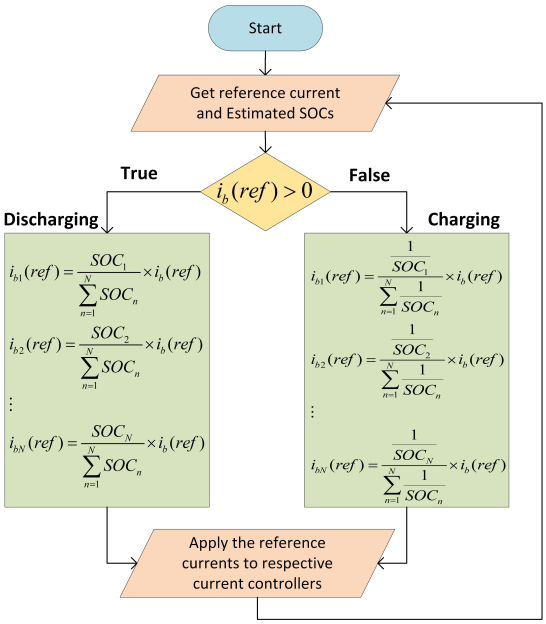

Fig. 5. Flowchart of reference current generation block

IV. Results and Discussions

The system shown in Figure 2 is simulated with the control scheme shown in Figure 4 and the system parameters stated in Table I. The reference voltage of DC bus is set to $120V$; irradiance is changing from from $1000W/m^2$ to $500W/m^2$ with a finite negative slope and again back to $1000W/m^2$with a finite positive slope. The load is changed in step at 2 seconds and 4 seconds. Regardless of changing load and irradiance, the DC bus voltage is maintained constant at $120V$ as shown in Figure 6.

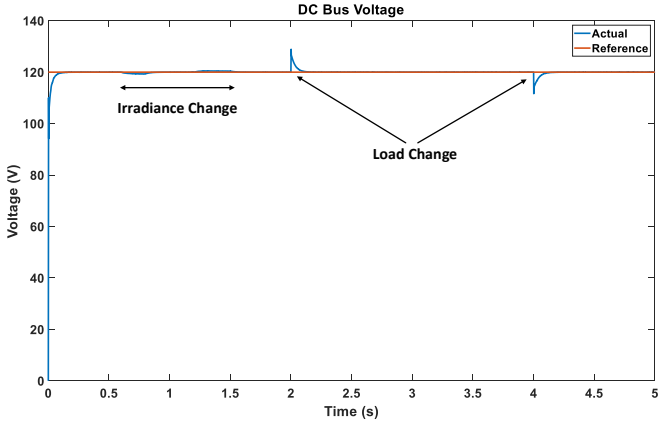

Fig. 6. DC bus voltage

The charging and discharging currents of the batteries are generated by reference current generation block according to their SOCs. The current sharing algorithm of the reference current generation block is shown in Figure 5. The battery with more SOC (in this case, its li-ion) would discharge at a higher rate and charge at a lower rate. Here, li-ion battery is at 80% SOC, and lead acid is at 40% SOC level. So, while discharging current from li-ion is double (proportional to its SOC) than current from lead acid, and while charging, lead acid is charging at a double rate than li-ion. Reference and actual currents from both batteries are shown in Figure 7. It is clearly observed that inner current controllers are working fine since actual currents are following the reference currents.

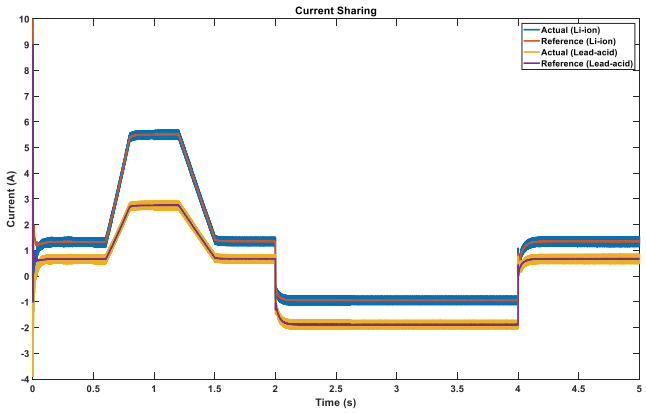

Fig. 7. Current sharing

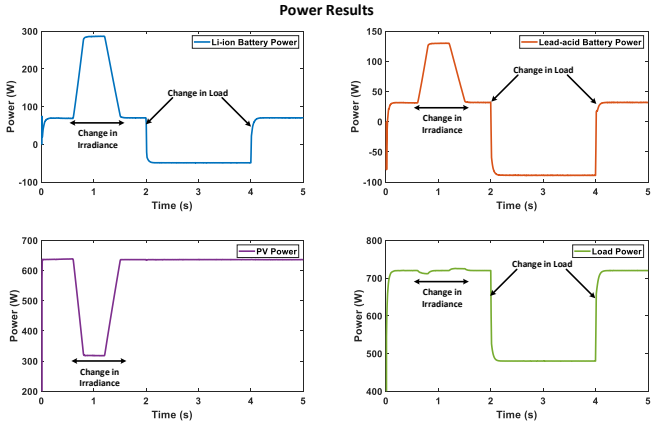

Fig. 8. Power sharing

Figure 8 shows power from PV, Li-ion battery, Lead-acid battery, and load. Change in irradiance results in a change in PV power. As power from PV decreases, power from batteries increases to maintain the DC bus voltage constant and fulfill the load requirement, sharing the discharge currents based on their SOCs. A step change in load at 2 seconds puts the batteries in charging mode, shown by the negative powers of the batteries. Charging current is also decided based on their SOCs.

V. Conclusions

This article discusses the integration of PV and multiple battery energy storage systems to a common DC bus through DC-DC converters. Averaged nonlinear model of the converter system consisting of a PV and two different BESSs is developed. The model is linearized around an operating point, and the linear model is validated by applying source voltage and duty cycle perturbations. A control scheme is discussed, which consists of an outer voltage controller, a centralized reference current generation block, and inner current controllers. Reference current generation scheme ensures the battery with more SOC would discharge at a higher rate and charge at a lower rate, and the opposite would be the case for the battery with lower SOC. Simulation studies have been performed in MATLAB/Simulink environment in varying irradiance and load conditions. PV is operating in MPPT mode using the P&O algorithm, and DC bus voltage is maintained constant using the outer voltage controller. Battery currents or inductor currents are controlled by inner current controllers at their reference values based on the SOCs of the batteries. The future work will include hardware validation of the proposed method.

Acknowledgment

The work is done under the project “Different Energy Vector Integration for Storage of Energy (DEVISE)” supported by the Department of Science and Technology (DST), Govt. of India under project grant no. TMD/CERI/MICALL19/ 2020/03(G).

APPENDIX A
FIRST APPENDIX

Operating point about which the system is linearized is $Q_{pv} = 0.279950951017653$, $Q_{b1} = Q_{b2} = 0.602478531176197$

$$\alpha_{pv} = -\left(R_s - R_p\right) I_{pv} + R_p Q'_{b1} I_{b1} + R_p Q'_{b2} I_{b2} + \frac{R_p V_c}{R_c} + V_D$$

$$\alpha_{b1} = -\left(R_s - R_p\right) I_{b1} + R_p Q'_{pv} I_{pv} + R_p Q'_{b2} I_{b2} + \frac{R_p V_c}{R_c} + V_D$$

$$\alpha_{b2} = -\left(R_s - R_p\right) I_{b2} + R_p Q'_{pv} I_{pv} + R_p Q'_{b1} I_{b1} + \frac{R_p V_c}{R_c} + V_D$$

TABLE I
SYSTEM PARAMETERS

System Parameters	Value
DC Bus Voltage (V_{bus})	$120V$
Maximum Power Point Voltage (V_{mp})	$87V$
Maximum Power Point (MPP) Power	$638W$
Nominal Voltage of Li-ion Battery (V_{b1})	$48V$
Ah Rating of Li-ion Battery	$200Ah$
Initial SOC of Li-ion Battery	80%
Nominal Voltage of Lead-acid Battery (V_{b1})	$48V$
Ah Rating of Lead-acid Battery	$200Ah$
Initial SOC of Lead-acid Battery	40%
L_{pv}	$1mH$
L_{b1}	$2mH$
L_{b2}	$2mH$
DC link Capacitance (C_{bus})	$100\mu F$
Switching Frequency (f_s)	$50kHz$

REFERENCES

[1] M. H. Saeed, W. Fangzong, B. A. Kalwar, and S. Iqbal, "A review on microgrid's challenges & perspectives," *IEEE Access*, vol. 9, pp. 166502–166517, 2021.

[2] M. G. Molina, "Energy storage and power electronics technologies: A strong combination to empower the transformation to the smart grid," *Proceedings of the IEEE*, vol. 105, no. 11, pp. 2191–2219, 2017.

[3] M. Stecca, L. R. Elizondo, T. B. Soeiro, P. Bauer, and P. Palensky, "A comprehensive review of the integration of battery energy storage systems into distribution networks," *IEEE Open Journal of the Industrial Electronics Society*, vol. 1, pp. 46–65, 2020.

[4] P. B. L. Neto, O. R. Saavedra, and L. A. de Souza Ribeiro, "A dual-battery storage bank configuration for isolated microgrids based on renewable sources," *IEEE Transactions on Sustainable Energy*, vol. 9, no. 4, pp. 1618–1626, 2018.

[5] C.-S. Moo, K. S. Ng, and Y.-C. Hsieh, "Parallel operation of battery power modules," *IEEE Transactions on Energy Conversion*, vol. 23, no. 2, pp. 701–707, 2008.

[6] K. D. Hoang and H.-H. Lee, "Accurate power sharing with balanced battery state of charge in distributed dc microgrid," *IEEE Transactions on Industrial Electronics*, vol. 66, no. 3, pp. 1883–1893, 2018.

[7] K. Thirugnanam, S. K. Kerk, C. Yuen, N. Liu, and M. Zhang, "Energy management for renewable microgrid in reducing diesel generators usage with multiple types of battery," *IEEE Transactions on Industrial Electronics*, vol. 65, no. 8, pp. 6772–6786, 2018.

[8] W. Wang, M. Zhou, H. Jiang, Z. Chen, and Q. Wang, "Improved droop control based on state-of-charge in dc microgrid," in *2020 IEEE 29th international symposium on industrial electronics (ISIE)*, pp. 1509–1513, IEEE, 2020.

[9] S. Kumari and S. Mishra, "Decentralized soc based droop with sliding mode current controller for dc microgrid," in *2018 5th IEEE Uttar Pradesh Section International Conference on Electrical, Electronics and Computer Engineering (UPCON)*, pp. 1–5, IEEE, 2018.

[10] B. R. Ravada and N. R. Tummuru, "Control of a supercapacitor-battery-pv based stand-alone dc-microgrid," *IEEE Transactions on Energy Conversion*, vol. 35, no. 3, pp. 1268–1277, 2020.

[11] M. Madadi and S. Bhattacharya, "Adaptive nonlinear droop control with dynamic state-of-charge balancing capability for batteries in dc microgrids," in *2021 IEEE Applied Power Electronics Conference and Exposition (APEC)*, pp. 55–61, IEEE, 2021.

[12] Y. Hong, D. Xu, W. Yang, B. Jiang, and X.-G. Yan, "A novel multi-agent model-free control for state-of-charge balancing between distributed battery energy storage systems," *IEEE Transactions on Emerging Topics in Computational Intelligence*, vol. 5, no. 4, pp. 679–688, 2020.

[13] N. Ghanbari, M. Mobarrez, and S. Bhattacharya, "A review and modeling of different droop control based methods for battery state of the charge balancing in dc microgrids," in *IECON 2018-44th Annual Conference of the IEEE Industrial Electronics Society*, pp. 1625–1632, IEEE, 2018.

[14] Y. Kim, V. Raghunathan, and A. Raghunathan, "Design and management of battery-supercapacitor hybrid electrical energy storage systems for regulation services," *IEEE Transactions on Multi-Scale Computing Systems*, vol. 3, no. 1, pp. 12–24, 2016.

[15] M. Chen and G. A. Rincon-Mora, "Accurate electrical battery model capable of predicting runtime and iv performance," *IEEE transactions on energy conversion*, vol. 21, no. 2, pp. 504–511, 2006.

[16] Y. Chen, P. Wang, H. Li, and M. Chen, "Power flow control in multi-active-bridge converters: Theories and applications," in *2019 IEEE Applied Power Electronics Conference and Exposition (APEC)*, pp. 1500–1507, IEEE, 2019.

[17] N. Mukherjee and D. Strickland, "Analysis and comparative study of different converter modes in modular second-life hybrid battery energy storage systems," *IEEE Journal of Emerging and Selected Topics in Power Electronics*, vol. 4, no. 2, pp. 547–563, 2015.

[18] J.-O. Lee, Y.-S. Kim, T.-H. Kim, and S.-I. Moon, "Novel droop control of battery energy storage systems based on battery degradation cost in islanded dc microgrids," *IEEE Access*, vol. 8, pp. 119337–119345, 2020.

[19] Q. Wu, R. Guan, X. Sun, Y. Wang, and X. Li, "Soc balancing strategy for multiple energy storage units with different capacities in islanded microgrids based on droop control," *IEEE journal of emerging and selected topics in power electronics*, vol. 6, no. 4, pp. 1932–1941, 2018.

[20] N. Ghanbari and S. Bhattacharya, "Soc balancing of different energy storage systems in dc microgrids using modified droop control," in *IECON 2018-44th Annual Conference of the IEEE Industrial Electronics Society*, pp. 6094–6099, IEEE, 2018.

[21] R. Hu and W. W. Weaver, "Dc microgrid droop control based on battery state of charge balancing," in *2016 IEEE Power and Energy Conference at Illinois (PECI)*, pp. 1–8, IEEE, 2016.